Optimization and Experimental Validation of Medium-Frequency High Power Transformers in Solid-State Transformer Applications

M. A. Bahmani and T. Thiringer
Chalmers University of Technology
Gothenburg, Sweden
Email: bahmani@chalmers.se
torbjorn.thiringer@chalmers.se

M. Kharezy
SP Technical Research Institute of Sweden
Borås, Sweden
Email: Mohammad.Kharezy@sp.se

***Abstract*—High power isolated DC-DC converters are likely to provide solutions for many technical challenges associated with power density, efficiency and reliability in potential applications such as offshore wind farms, inter-connection of DC grids, MVDC in data centers and in future solid state transformer applications. The high power medium frequency transformer (HPMFT) is one of the key elements of such a converter to realize the voltage adaption, isolation requirements, as well as high power density. This paper describes a design and optimization methodology taking into account the loss calculation, isolation requirements and thermal management. Incorporating this design methodology, an optimization process with a wide range of parameter variations is applied on a 50 kW, 1 / 3 kV, 5 kHz transformer to find the highest power density while the efficiency, isolation, thermal and leakage inductance requirements are all met. The optimized transformers are then manufactured and will be presented in this paper.**

I. Introduction

Nowadays, power electronic converters are considered as one of the enabling technologies that can address many technical challenges in future power grids from the generation phase to the transmission and consequently distribution at different voltage levels [1]. In contrast to the medium power converters (5 to 100 kW) which have been essentially investigated in automotive and traction applications, the megawatt and medium voltage range isolated converters with several kilohertz isolation stage are still mainly in an expansive research phase [2].

Under the scope of grid applications, one of the most cited terminologies for these kinds of high power converters is called solid-state transformer (SST) which is in fact an AC-AC or DC-DC high power converters whereby the voltage adaptation and high-frequency isolation, to reduce the weight and volume, are achieved. Medium-frequency or high-frequency power transformer (MFPT/HFPT) are numerously cited as the key element of SSTs [3] which can potentially replace the conventional LF transformers. The main requirements of SSTs, i.e., high power density, lower specific losses, voltage adaptation and isolation requirements are entirely or to a great extent fulfilled through a careful design of medium frequency transformers.

However, taking high power, high voltage and high frequency effects into account, there are several challenges to be addressed. These challenges are basically related to the extra losses as a result of eddy current in the magnetic core, excess losses in the windings due to enhanced skin and proximity effects [4] and parasitic elements, i.e., leakage inductance and winding capacitances, causing excess switching losses in the power semiconductors which are usually the dominant power losses at higher frequencies [5]. These extra losses together with the reduced size of the transformer lead to higher loss densities requiring a proper thermal management scheme in order to dissipate the higher power losses from a smaller component.

Utilizing a set of more accurate loss evaluation methods, this paper presents a design methodology addressing the applicability of rectangular litz conductors, the high isolation requirements of offshore based transformers as well as the required inductance of the dual active bridge (DAB) topology. In the proposed design, the aforementioned inductance is integrated within the medium frequency transformer as its leakage inductance as shown in Fig. 1. Utilizing this design methodology, an optimization process with a wide range of parameter variations is performed to get the highest power density while the efficiency, isolation, thermal and leakage inductance requirements are all met [6]. Using the proposed design and optimization approach, two optimized 50 kW, 1 / 3 kV, 5 kHz medium frequency transformers have been designed and manufactured. This paper describes different steps in order to design, optimize and validate the mentioned prototype.

II. DC-DC Converter Topology

Recently, there has been growing interest in utilizing dual Active bridge (DAB) converters in high power applications. The equivalent circuit of a DAB converter is shown in Fig. 1(a) in which two square wave voltage waveforms on the two sides of the transformer has been shifted by controlling the input and output bridges, applying full voltage over the inductance, L_σ, which is used to shape the current as a power transfer element [7]. The steady state transformer voltage and current waveforms of a DAB converter with simple phase shift modulation are shown in Fig. 1(b). It is worth to point out that in order to have soft switching at turn on, the anti-parallel diode of each switch should start conducting prior to the turn on moment. In order to achieve zero voltage switching (ZVS)

978-1-4673-9550-2/16/$31.00 ©2016 IEEE

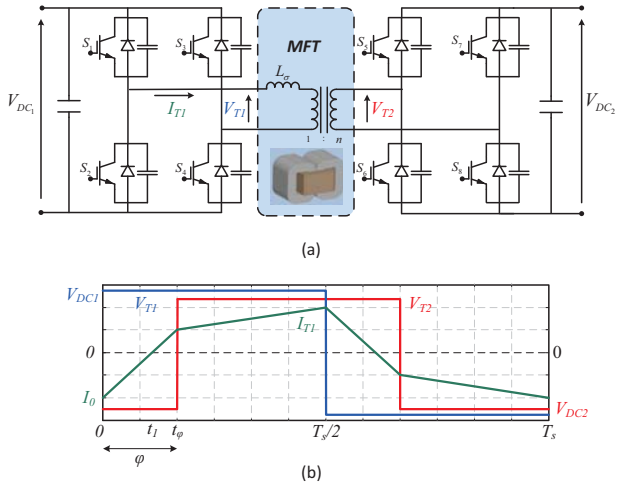

Fig. 1: (a) Dual active bridge circuit. (b) Steady state medium frequency transformer voltage and current waveforms

at turn on, the phase shift between the bridges, φ, should be higher than a certain value resulting in a minimum value of the series inductance as presented in (1). This inductance is preferably integrated as the leakage inductance of the medium frequency transformer, Fig. 1(a), in order to reduce the number of components, hence achieving higher power densities.

$$L_{\sigma(min)} = \frac{V_{DC_1} V_{DC_2} \varphi_{min}(\pi - \varphi_{min})}{2P_{out}\pi^2 f_s n} \tag{1}$$

where φ_{min} which is associated with the worst case condition, in which the maximum output voltage deviation occurs, can be calculated as.

$$\begin{aligned} \varphi_{min} &= \frac{\pi\,(d-1)}{2d} \quad for \quad d > 1 \\ \varphi_{min} &= \frac{\pi\,(1-d)}{2} \quad for \quad d < 1 \end{aligned} \tag{2}$$

and d, the DC conversion ratio for the worst case condition, is defined as

$$d = \frac{V_{DC2}(worst\ condition)}{nV_{DC1}}. \tag{3}$$

It should be noted that in normal conditions, d equals 1. The waveforms illustrated in Fig. 1(b) will later, in this paper, be used as the transformer excitations and consequently they will affect the transformer losses, i.e, copper and core losses.

III. Optimization Procedure

Fig. 2 shows the proposed optimization flowchart used for designing a medium frequency high power transformer which is supposed to meet the mentioned requirements. Different parts of this design and optimization process are explained in details below.

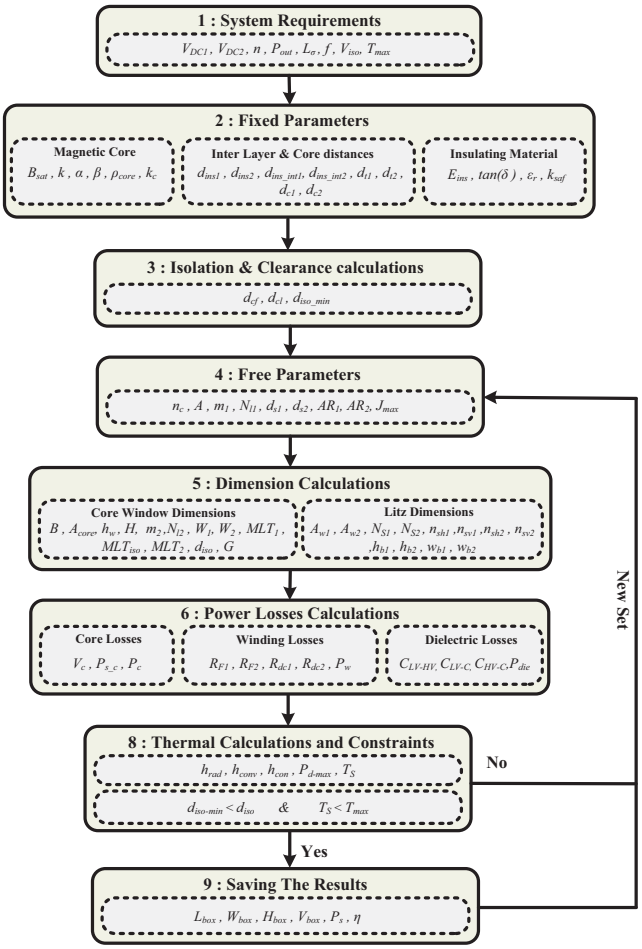

Fig. 2: Design Algorithm.

A. System Requirements and Considerations

The first step is to introduce the converter level requirements, i.e, output power, P_{out}, DC voltage levels, V_{DC1} and V_{DC2}, operating frequency, f, transformer turn ratio, n, required leakage inductance, L_σ, and isolation requirements, V_{iso}, as well as the maximum operating temperature T_{max}. The transformer is exposed to the voltage and current waveforms shown in Fig. 1(b) as the typical waveforms of a DAB converter. However, the proposed design methodology can easily be applied on other types of modulations with duty cycles, D_1 and D_2, being below 0.5. It is worth to point out that because of the power rating limitations of modern semiconductor devices, a modular concept comprising of building blocks enabling parallel connection on the low voltage side and series connection on the high voltage side, will most likely be considered [8], particularly in high power and high voltage applications.

B. Fixed Parameters

Prior to the iterative optimization part, the magnetic core material, insulation material, the windings type and inter-layer distances need to be set.

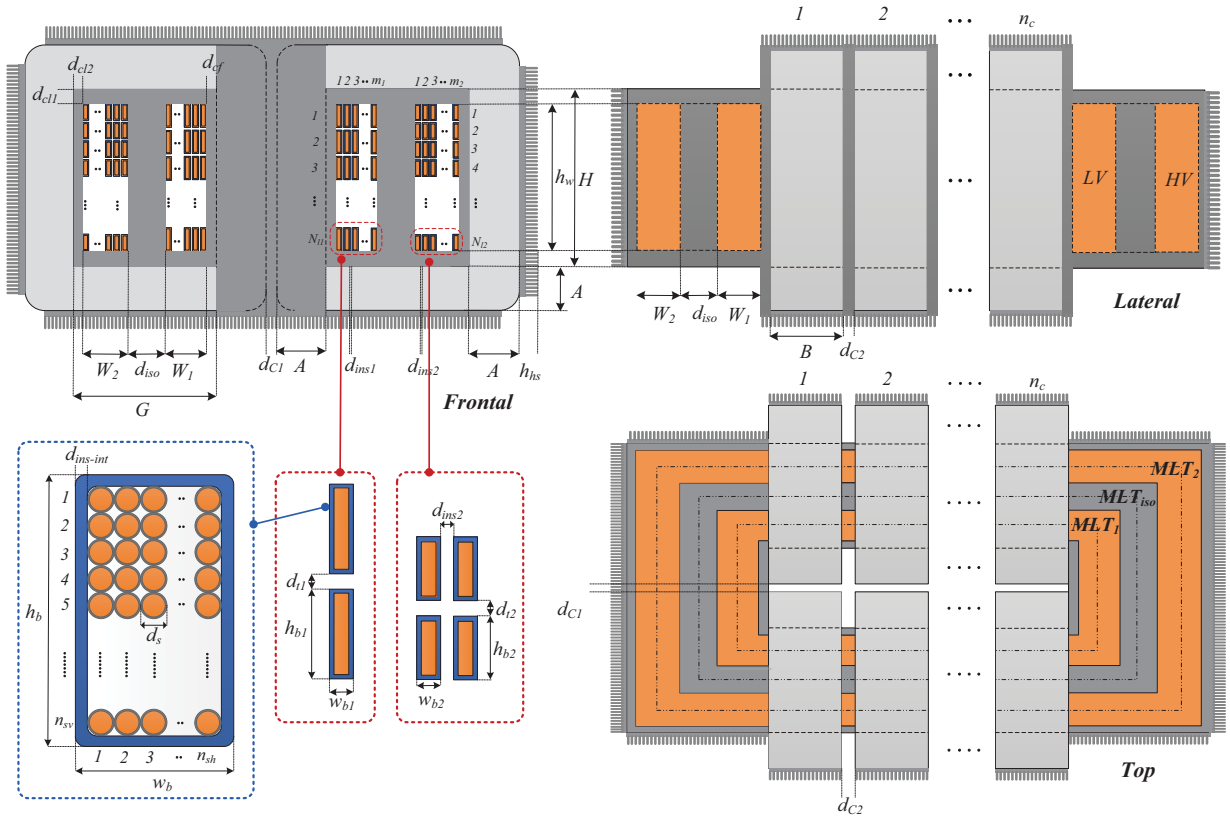

Fig. 3: Design sketch.

C. Free Parameters

For the purpose of this study, nine free parameters which are swept over a wide range are designated as the number of the magnetic core stacks, n_c, the frontal side of the core cross section, A, the number of layers and the number of litz bundle turns per layer in the primary windings portion, m_1 and N_{l1}, the diameter of the strands in the primary and secondary litz wires, d_{s1} and d_{s2}, the aspect ratios of the primary and secondary litz bundles which is the ratio between the respective total height and width, AR_1 and AR_2, and finally the maximum allowed RMS value of the current density through a conductor, J_{max}. The selection of free parameters highly depends on the optimization targets and restrictions, as well as the considered core and winding topologies. For instance, in case of foil conductors, one can consider the thickness of the foil conductors as the complementary free parameter.

All possible combinations of these free parameters will be applied to the optimization flowchart shown in Fig. 2, resulting in distinct transformer geometries corresponding to its set of free variables. Utilizing the modified and developed expressions, the core, windings and dielectric losses are then being evaluated for each set of free parameters [9], [10]. The efficiency, power density and temperature rise of each transformer are then extracted and compared in order to obtain the optimum combination that meets the requirements.

D. Geometry Determination

Having the fixed and free parameters, the transformer geometry can be defined as follows. First, the required magnetic core cross section is defined as

$$A_c = \frac{V_{DC1}}{\frac{2\sqrt{2D-\frac{8}{3}R}}{D-R} k_c m_1 N_{l1} B_m f}. \tag{4}$$

Considering the geometry structure shown in Fig. 3 and considering the number of core stacks, n_c, the lateral side length of the magnetic core can be calculated as

$$B = \frac{A_c}{2n_c A} \tag{5}$$

where A is the frontal side length of each core stack. With a specific set of strand diameters and the allowed current density given by the free parameters, the number of strands at the primary and secondary litz bundles can be respectively calculated as

$$N_{s1} = \left\lceil \frac{4I_{T1}}{\pi d_{s1}^2 J_{max}} \right\rceil \quad , \quad N_{s2} = \left\lceil \frac{4I_{T1}}{n\pi d_{s2}^2 J_{max}} \right\rceil \tag{6}$$

where I_{T1}, the transformer primary RMS current, is the function of the applied phase shift, φ, which is in this case the minimum allowed value ensuring the soft switching and

yet having a reasonable amount of reactive power circulation. On the basis of the waveforms presented in Fig. 1(b), I_{T1} can be calculated from

$$I_{T1}\,(rms) = Z\sqrt{\frac{4t_1^2 t_\varphi + T_s t_1^2 - 4t_\varphi^2 t_1 - T_s t_1 t_\varphi + T_s t_\varphi^2}{3T_s}} \tag{7}$$

where Z, t_1 and t_φ are respectively calculated by

$$Z = \frac{nV_{DC1} + V_{DC2}}{nL_\sigma} \tag{8}$$

$$t_1 = \frac{\pi + 2\varphi d - \pi d}{4\pi f\,(1+d)} \quad , \quad t_\varphi = \frac{\varphi}{2\pi f}. \tag{9}$$

After determining the number of strands in each litz bundle, the number of strands in each internal row of the litz bundle, n_{sh} as shown in Fig. 3 , can be calculated by (10) as

$$n_{sh} = \left\lfloor \frac{k + \sqrt{k^2 + N_s d_s^2.AR}}{d_s.AR} \right\rfloor \tag{10}$$

where k is

$$k = d_{ins-int}(1 - AR). \tag{11}$$

It should be pointed out that (10) and (11) are used for both the primary and secondary windings, n_{sh1} and n_{sh2}, with their corresponding free parameters. This internal arrangement of the litz bundle will be later used to calculate the winding losses. Accordingly, the number of strands in each internal column within a litz bundle of primary and secondary windings, with corresponding free parameters, can be defined by

$$n_{sv1} = \left\lceil \frac{N_{s1}}{n_{sh1}} \right\rceil \quad , \quad n_{sv2} = \left\lceil \frac{N_{s2}}{n_{sh2}} \right\rceil. \tag{12}$$

As a result, the winding height, h_w, the core window height, H, and the primary windings build are respectively calculated as

$$h_w = (N_{l1} + 1)\,(n_{sv1} d_{s1} + 2d_{ins-int1}) + N_{l1} d_{t1} \tag{13}$$

$$H = h_w + 2d_{cl} \tag{14}$$

$$W_1 = m_1(n_{sh1} d_{s1} + 2d_{ins-int1}) + (m_1 - 1) d_{ins1} \tag{15}$$

where d_{t1}, d_{ins1}, $d_{ins-int1}$ and other parameters were already illustrated in Fig. 3. Hence, the mean length turn of the primary windings, MLT_1, which will be later used for the windings loss calculation is obtained from

$$MLT_1 = 2\,(2A + d_{c1} + 4d_{cf} + n_c B + (n_c - 1)\,d_{c2} + 2W_1)\,. \tag{16}$$

Likewise, the number of turns per layer and the number of layers at the secondary litz winding are respectively calculated by

$$N_{l2} = \left\lfloor \frac{h_w - (n_{sv2} d_s + 2d_{ins-int2})}{(n_{sv2} d_s + 2d_{ins-int2}) + d_{t2}} \right\rfloor \tag{17}$$

$$m_2 = \left\lceil \frac{n m_1 N_{l1}}{N_{l2}} \right\rceil. \tag{18}$$

Accordingly, the secondary winding build is calculated from

$$W_2 = m_2\,(n_{sh2} d_{s2} + 2d_{ins-int2}) + (m_2 - 1)\,d_{ins2}. \tag{19}$$

1) Isolation Distance, d_{iso} : In order to be able to calculate the rest of the geometrical dimensions, i.e, the core window width, the total length and width of the transformer box and consequently the total volume of the box, one first needs to calculate the required isolation distance, d_{iso}, fulfilling the minimum isolation requirements, V_{iso}, as well as providing the desired leakage inductance, L_σ, ensuring the ZVS operation of the DC-DC converter.

For this purpose, the analytical expression presented in [10], accounting for the high frequency effect on the leakage inductance value, is rearranged as

$$d_{iso} = \frac{-8k_1 - k_2 m_1 + \sqrt{(k_2 m_1 + 8k_1)^2 - 16k_3 m_1}}{8m_1} \tag{20}$$

where k_1 to k_3 can be calculated according to the expressions presented in [6] for the foil and round conductors. However, in case of the rectangular litz wire used in this article, those coefficients should be adapted as follows

$$\begin{aligned} k_1 = {} & \frac{m_1(m_2-1)(2m_2-1)}{6m_2} d_{ins2} \\ & + \frac{m_1'}{m_2'} \frac{sin(\frac{2\Delta_2}{\alpha\delta})4\alpha\delta^2({m_2'}^2 - 1) + 4d_{s2}'(2{m_2'}^2 + 1)}{24sin^2(\frac{2\Delta_2}{\alpha\delta}))} \\ & + \frac{m_1'}{m_2'} \frac{-\alpha\delta^2 sin(\frac{4\Delta_2}{\alpha\delta})(2{m_2'}^2 + 1) + 8d_{s2}'(1 - {m_2'}^2)cos(\frac{2\Delta_2}{\alpha\delta})}{24sin^2(\frac{2\Delta_2}{\alpha\delta}))} \end{aligned} \tag{21}$$

where the number of layers, strand diameters and the penetration ratios are adapted for the rectangular litz conductor as

$$m_1' = n_{sh1} m_1 \quad , \quad m_2' = n_{sh2} m_2 \tag{22}$$

$$d_{s1}' = d_{s1}\frac{\sqrt{\pi}}{2} \quad , \quad d_{s2}' = d_{s2}\frac{\sqrt{\pi}}{2} \tag{23}$$

$$\Delta_1 = \frac{d_{s1}}{2\delta}\sqrt{\frac{\pi N_{l1} n_{sv1} d_{s1}\sqrt{\pi}}{2H}}\,,\ \Delta_2 = \frac{d_{s2}}{2\delta}\sqrt{\frac{\pi N_{l2} n_{sv2} d_{s2}\sqrt{\pi}}{2H}} \tag{24}$$

where δ is the skin depth at any particular frequency and α is defined as $\frac{1+j}{\delta}$. Furthermore, k_2 can be calculated as

$$k_2 = MLT_1 + 4W_1 \tag{25}$$

and k_3 are calculated as

$$k_3 = (MLT_1 + 4(W_1 + W_2))k_1 - k_4 \tag{26}$$

where k_4 with the rectangular litz conductor's parameters can be calculated as

$$\begin{aligned} k_4 = & \frac{h_w}{\mu m_1 N_{l1}^2} L_{\sigma 1} \\ & - MLT_1 \frac{(m_1 - 1)(2m_1 - 1)}{6} d_{ins1} \\ & - MLT_1 \frac{sin(\frac{2\Delta_1}{\alpha\delta})4\alpha\delta^2(m_1'^2 - 1) + 4d'_{s1}(2m_1'^2 + 1)}{24sin^2(\frac{2\Delta_1}{\alpha\delta}))} \\ & + MLT_1 \frac{\alpha\delta^2 sin(\frac{4\Delta_1}{\alpha\delta})(2m_1'^2 + 1) - 8d'_{s1}(1 - m_1'^2)cos(\frac{2\Delta_1}{\alpha\delta})}{24sin^2(\frac{2\Delta_1}{\alpha\delta}))} \end{aligned} \tag{27}$$

Thus, the expression in (20) gives the required isolation distance providing the desired leakage inductance as one of the design specifications. It should be noted that the obtained value of d_{iso} must be sufficient enough to withstand the isolation voltage level, V_{iso}. Otherwise, the design is not acceptable and the next transformer geometry construction with a new set of the free parameters will be initiated.

Having V_{iso} determined, one can uniquely draw the transformer sketch, shown in Fig. 3, with all the geometrical details. Therefore, it is possible to utilize the loss evaluation methods, in order to calculate the power losses of each transformer corresponding to each set of free parameters.

E. Losses Calculations

The magnetic components volume reduction at higher frequencies is at the expense of enhanced core losses as well as increased winding losses due to intensified skin and proximity effects. Although the main focus is to mitigate this loss enhancement by utilizing the proper magnetic material, winding type as well as the right thermal management strategy, it is also important to more accurately evaluate the aforementioned power losses in order to properly implement a thermal management scheme. For this purpose, various analytical and empirical loss evaluation methods have been studied and modified in some cases. Finally the most suitable ones have been selected to be used in this paper.

1) Core Losses: In order to evaluate the core losses, the modified expression of the improved generalized Steinmetz equation (IGSE) adapted for the square-wave excitation with arbitrary duty cycles and rise times presented in [6] has been used as

$$P_{core} = \left(2D - \frac{4\alpha}{\alpha + 1} R\right) \frac{2^\beta}{(D - R)^\alpha} k.k_i f^\alpha B_m^\beta V_c \rho \tag{28}$$

where D and R are equal to 0.5 and 0 respectively for the standard phase shift DAB converter, ρ is the magnetic core density, α and β are the Steinmetz core loss coefficients. Moreover, the coefficient, k_i, which is a function of α and β can be calculated as

$$k_i = \frac{1}{(2\pi)^{\alpha-1} \int_0^{2\pi} |cos(\theta)|^\alpha \, 2^{\beta-\alpha} d\theta} \tag{29}$$

Accordingly, the magnetic core volume, V_c, can be determined as follows

$$V_c = 4n_c AB\,(H + 2A) + 4n_c ABG \tag{30}$$

in which H is the window height previously calculated in (14) and G is the core window width calculated from

$$G = d_{cf} + W_1 + d_{iso} + W_2 + d_{cl} \tag{31}$$

2) Windings Losses : The winding losses can be calculated using the harmonic contents of the excitation current, thus

$$P_{w1} = \sum_{h=1}^{n} R_{DC1}.RF_{1_h}.I_{1_h}^2 \quad , \quad P_{w2} = \sum_{h=1}^{n} R_{DC2}.RF_{2_h}.I_{2_h}^2 \tag{32}$$

where R_{DC1} and R_{DC2} are the DC resistance of the primary and secondary windings portion, RF_{1_h} and RF_{2_h} are respectively the AC resistance factor of the primary and secondary windings portion at the h^{th} harmonic. In addition, I_{1_h} and I_{2_h}, are respectively the rms values of the primary and secondary currents through the transformer windings for the h^{th} harmonic. The DC resistance of the primary and secondary windings portion associated with rectangular litz winding arrangement shown in Fig. 3 are calculated from

$$R_{DC1} = \frac{4m_1 N_{l1} MLT_1}{\sigma\pi d_{s1}^2 N_{s1}} \quad , \quad R_{DC2} = \frac{4m_2 N_{l2} MLT_2}{\sigma\pi d_{s2}^2 N_{s2}} \tag{33}$$

where σ is the conductivity of the conductors, here copper, MLT_1 is previously defined in (16) and MLT_2 is the mean length turn of the secondary winding which is calculated, as can be seen in top view of Fig. 3, as

$$MLT_2 = MLT_1 + 4W_1 + 4W_2 + 8d_{iso}. \tag{34}$$

As shown in Fig. 1(b), the transformer voltages and currents are not sinusoidal. Therefore, AC resistance factors, RF_{1_h} and RF_{2_h}, should be, separately for each harmonic content, calculated from the expression in [11] which, in this paper, is adapted to account for the rectangular litz configuration shown in Fig. 3.

$$\begin{aligned} RF\,(\Delta_h) = & \Delta_h \left(\frac{sinh(2\Delta_h) + sin(2\Delta_h)}{cosh(2\Delta_h) - cos(2\Delta_h)}\right) \\ & + \frac{2\Delta_h(m^2 n_{sh}^2 - 1)}{3} \left(\frac{sinh(\Delta_h) - sin(\Delta_h)}{cosh(\Delta_h) + cos(\Delta_h)}\right) \end{aligned} \tag{35}$$

where Δ_h is the penetration ratio of the h^{th} harmonic defined in (24) in which, it is clear that Δ_h increases at higher harmonic numbers, because it is inversely proportional to the skin depth.

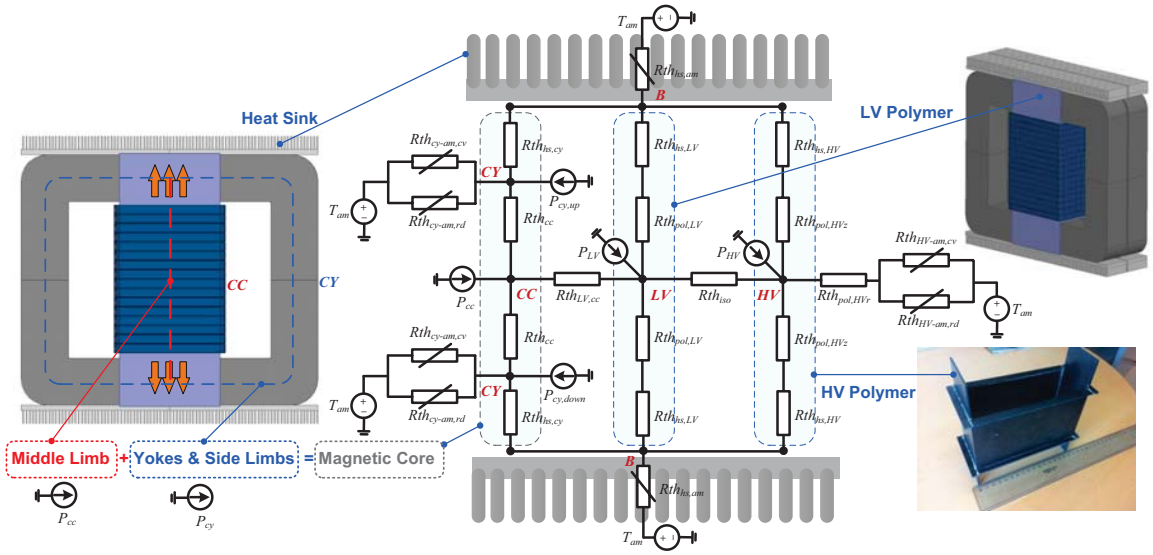

Fig. 4: Equivalent thermal network of the proposed transformer topology with six temperature nodes, i.e, (a) HV winding temperature, T_{HV} (b) LV winding temperature, T_{LV} (c) Center limb core temperature, T_{cc} (d) Yokes and side limbs temperature, T_{cy} (e) heat sink base temperature, T_b and (f) Ambient temperature, T_{am} .

Finally, the rms value of the h^{th} harmonic of the transformer currents, to be used in (32), are derived as

$$I_{1_h} = \frac{4V_{DC1}\sqrt{1+d^2-2dcos(h\varphi)}}{2\sqrt{2}\pi^2 f h^2 L_\sigma} \quad , \quad I_{2_h} = \frac{I_{1_h}}{n} \tag{36}$$

F. Thermal Analysis

The combination of two thermal management methods, shown in Fig. 4, are implemented in the current design approach. First of all, as in planar transformers, heat sinks are considered to be placed on the core surfaces in order to increase the effective surface area resulting in thermal resistance reduction and consequently higher power dissipation capability of the design. The main drawback of this method, besides increasing the total volume of the transformer box, is that due to the poor thermal contact of the core and the primary windings, the heat around the middle limbs, usually the hottest spot of the transformer, can not easily be conducted to the heat sink. For this reason, a complementary thermal management method has been incorporated placing a thermally conductive material between the primary windings and the core in order to directly conduct the heat to the top and bottom part of the transformer where heat sinks are assembled.

The equivalent thermal network of the proposed transformer is depicted in Fig. 4 in which six different temperature nodes connected by the thermal resistances have been considered. These temperature nodes are the HV winding temperature, T_{HV}, LV winding temperature, T_{LV}, center limb core temperature, T_{cc}, yokes and side limbs temperature, T_{cy}, heat sink base temperature, T_b and finally the ambient temperature, T_{am}. In shell type transformers the middle limb is surrounded by the windings. Hence its surfaces are not exposed to the air and its corresponding heat should be first conducted to the surface areas which are exposed to the open air and then be dissipated by means of convection and radiation. Therefore, the magnetic core is divided into two areas, the middle limb with the temperature, T_{cc}, and the rest of the core consisting of side limbs and the yokes with the temperature, T_{cy}. The main assumption here is that each of the aforementioned sections are assumed to have a uniform temperature distribution, e.g., all copper areas inside the LV winding portion is assumed to have a one temperature, T_{LV}.

It should be mentioned that the heat exchange inside the transformer is mainly taking place due to the heat conduction mechanism, whereas the outer parts, the heat sinks and the open surfaces, transfer heat to the surrounding fluid, air, by means of convection and radiation mechanisms. Therefore, the thermal resistances illustrated in Fig. 4 are composed of conduction thermal resistances, as well as the convection and radiation ones. These thermal resistances are here calculated with respect to the transformer design sketch shown in Fig. 3.

Identifying the thermal network of the proposed design and calculating its corresponding thermal resistances, one can generally define the matrix representation as

$$AT + BU = 0 \Rightarrow T = -A^{-1}BU \tag{37}$$

where the matrices , T, U and B can be respectively represented as

$$T = \begin{bmatrix} T_{HV} \\ T_{LV} \\ T_{cc} \\ T_{cy} \\ T_B \end{bmatrix}_{5\times 1} \quad , \quad U = \begin{bmatrix} P_{HV} \\ P_{LV} \\ P_{cc} \\ P_{cy} \\ P_B \\ T_{am} \end{bmatrix}_{6\times 1} \tag{38}$$

TABLE I: Design specification of the prototypes

Output Power, P_{out}	50 kW
Low voltage side, V_{LV}	1 kV
High voltage side, V_{HV}	3 kV
Leakage inductance, L_σ	38 and 29 μH
Transformer turn ratio, n	3
Isolation level, V_{iso}	6 kV
Switching frequency, f	5 kHz

$$B = \begin{bmatrix} 1 & 0 & 0 & 0 & 0 & \frac{1}{R_{th_{pol,HVr}} + R_{th_{HV,am}}} \\ 0 & 1 & 0 & 0 & 0 & 0 \\ 0 & 0 & 1 & 0 & 0 & 0 \\ 0 & 0 & 0 & 1 & 0 & \frac{2}{R_{th_{cy,am}}} \\ 0 & 0 & 0 & 0 & 0 & \frac{2}{R_{th_{hs,am}}} \end{bmatrix}_{5\times 6} \tag{39}$$

and A can be presented by

$$A = \begin{bmatrix} R_1 & \frac{1}{R_{th_{iso}}} & 0 & 0 & \frac{2}{R_{th_{HV_z}}} \\ \frac{1}{R_{th_{iso}}} & R_2 & \frac{1}{R_{th_{LV,cc}}} & 0 & \frac{2}{R_{th_{LV_z}}} \\ 0 & \frac{1}{R_{th_{LV,cc}}} & R_3 & \frac{2}{R_{th_{cc}}} & 0 \\ 0 & 0 & \frac{2}{R_{th_{cc}}} & R_4 & \frac{2}{R_{th_{hs,cy}}} \\ \frac{2}{R_{th_{HV_z}}} & \frac{2}{R_{th_{LV_z}}} & 0 & \frac{2}{R_{th_{hs,cy}}} & R_5 \end{bmatrix} \tag{40}$$

Unlike the conduction heat transfer coefficient, the convection and radiation heat transfer coefficients are strongly temperature dependent. Therefore, the matrix equation in (37) should be solved iteratively to achieve the steady state temperature of each node. The iterations start with the initial temperature as the ambient temperature for all the nodes and continue with the updated thermal resistances in each iteration until it yields the steady state value.

IV. Down-Scaled Prototype Design and Optimization

To validate the proposed design approach, two down-scaled 50 kW, 1 / 3 kV, 5 kHz medium frequency transformer prototypes with two different core material, i.e., nanocrystalline material, Vitroperm500F, and the ferrite, N87, have been designed and manufactured. The specification of the prototypes are tabulated in Table. I. The transformer prototypes are designed to operate with the voltage and current waveforms shown in Fig. 1(b) which are the typical waveforms of a DAB converter, although, the proposed design methodology can easily be applied on other types of modulations with duty cycles, D_1 and D_2, being below 0.5. The isolation level, 6 kV, is considered to account for two times the voltage of the high voltage side. The desired values of the leakage inductances are on the basis of maximum 4% and 3% output voltage deviation for the prototypes with N87 and Vitroperm500F, respectively.

A. Design and Optimization Results

The proposed design methodology explained in this article has been applied on the prototype specification shown in Table. I. For this purpose, each free parameter, shown in the forth step in Fig. 2, is swept over a wide range resulting in more than 400000 different combination of free parameters. Each unique combination of free parameters corresponds to a unique transformer geometry based on the design approach explained in this article. The great majority of the considered cases are discarded since they do not fulfill either the thermal requirements or the isolation distances required to obtain the desired leakage inductance. All the dimensional and electrical data of the remaining passed transformers are then saved, step 9 in Fig. 2, and will be used to form the Pareto-front optimization curve and consequently to choose the optimum point.

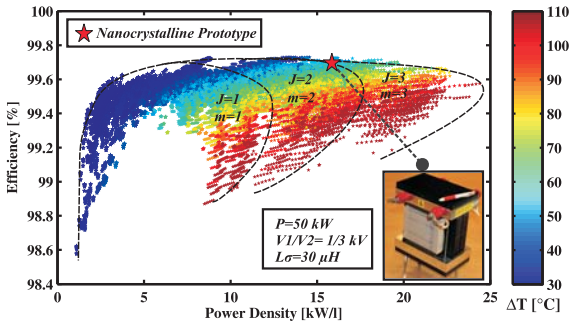

Fig. 5: Efficiency versus Power density of feasible nanocrystalline-based transformers according to the proposed design methodology.

The optimization outcome showing the efficiencies and power densities of the nanocrystalline based transformers corresponding to the accepted sets of free parameters illustrated in Fig. 5 in which each colored star represents a distinct transformer which meet all the design requirements and its color indicates the corresponding temperature rise of that particular transformer. The effect of the maximum allowed current density, J_{max}, and the number of primary layers, m_1, as two of the optimization free parameters are illustrated in Fig. 5. It can be seen that the achieved power densities increases by allowing higher current densities and number of winding layers; however, this is on the expense of higher loss densities and consequently higher temperature increase as one of the design constraints. The approximate borders between different J_{max} and m_1 are drawn in Fig. 5.

The nanocrystalline-based transformer design is highlighted in Fig. 5 with the large red star. According to the design approach, it is expected to reach a power density of 15.1 kW/l and the efficiency of 99.67%. These quantities will be evaluated on the manufactured prototype in the next parts of this article. The reason that the highest achievable power density is not selected for manufacturing the prototype, is that the author had limited selection of magnetic core dimensions, particularly for the nanocrysstalline prototype, as well as the limited dimensions of rectangular litz conductors which are available on the market. Similarly, the optimation outcome and the selected prtotype design of the Ferrite based transformers are shown in Fig. 6 in which the selected design, highlighted with a large red star, is expected to exhibit 99.54% efficiency while the power density is about 11.5 kW/l.

As stated before, two different types of magnetic material, i.e., Vitroperm500F and N87, are used to design and manufacture the prototype transformers. Both noncrystalline and Ferrite material are suitable for high frequency applications and it can be of interest to investigate their performance on two transformer prototypes with the same specifications. As can be seen in Fig. 5 and Fig. 6, Vitroperm500F demonstrates higher efficiencies for the same power density which can be explained by the lower specific losses of Vitroperm500F compared to N87. Furthermore, Fig. 5 and Fig. 6 show that Vitroperm500F based designs at 5 kHz can achieve substantially higher power densities of up to about 23 kW/l with maximum 70°C temperature increase compared to the one of about 13 kW/l for N87. This also can be explained by the relatively higher saturation level of Vitroperm500F compared to the one with N87 ferrite core. It is worth to mention that the high isolation requirements of the case study

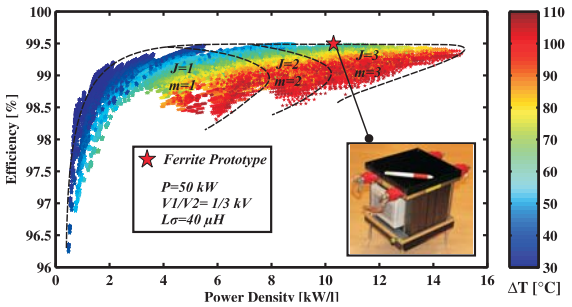

Fig. 6: Efficiency versus Power density of feasible ferrite-based transformers according to the proposed design methodology.

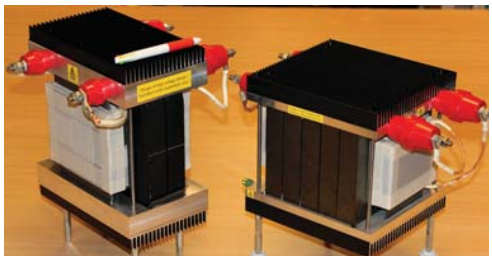

Fig. 7: Built prototypes

transformer, 6 kV isolation for a 3/6 kV transformer, together with the desired leakage inductance as two of the design inputs, play an important role in determining the power density of the final optimum design. The finally built nanocrystalline and ferrite-based transformer prototypes are presented in Fig. 7 in which the relatively smaller volume of the nanocrystalline-based prototype is clear.

B. Experimental Verification

The prototypes are exposed to extensive open and short circuit measurements for core and winding loss evaluations, respectively. The total expected losses of the nanocrystalline-based transformer is 166.1 W with the expected efficiency of 99.67%. The measurement results indicate a power loss of 176.1 W with the corresponding efficiency of 99.66%. The ferrite-based transformer is expected to have the efficiency of 99.52% with 241.5 W power losses. The experimental results showed 99.48% efficiency with the total power losses of 259.8 W. In order to measure the core losses, the actual waveform of the transformer has been applied on the LV side of the prototype under the test while the HV side was open. The voltage waveform, as well as the

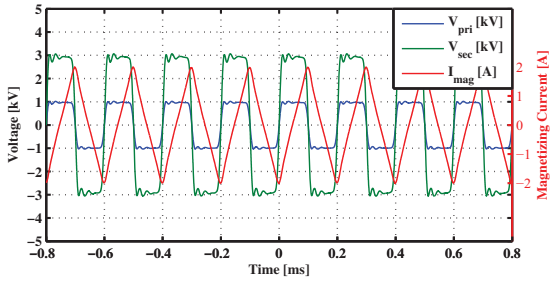

Fig. 8: Open circuit voltages and current waveforms used for the core loss measurements at 5 kHz.

corresponding magnetizing current is shown in Fig. 8. The measured leakage inductance of the nanocrystalline-based transformer is 29.9 μH which is only 3% higher than the intended design value, i.e, 29 μH. In case of the ferrite-based transformer, the design target of the leakage inductance was 38 μH while the measurement shows 40 μH which is a 5% deviation from the initial target.

V. Conclusions

This paper presented a design and optimization method for medium-frequency transformers in SST applications. Tuned value of the leakage inductance, high isolation requirements, applicability of the square-type litz conductors and nanocrystalline magnetic materials are different design aspects addressed in the proposed approach. Utilizing the proposed design method, two down-scaled prototype transformers have been design and manufactured. The nanocristalline-based prototype reached an efficiency of 99.66% which is almost the same as the theoretically predicted one. Also their leakage inductance were rather accurately predicted with the theoretical designs compared to the measured values.

Acknowledgment

Thanks to the Swedish Energy Agency for the financial support of this research. The authors would also like to thank Dr. Lars Kvarnsjö from VAC for providing us with the Vitroperm500F cores.

References

[1] K. Vechalapu, A. Kadavelugu, and S. Bhattacharya, "High voltage dual active bridge with series connected high voltage silicon carbide (sic) devices," in *Energy Conversion Congress and Exposition (ECCE), 2014 IEEE*, Sept 2014, pp. 2057–2064.

[2] M. Bahmani, T. Thiringer, A. Rabiei, and T. Abdulahovic, "Comparative study of a multi-mw high power density dc transformer with an optimized high frequency magnetics in all-dc offshore wind farm," *Power Delivery, IEEE Transactions on*, vol. PP, no. 99, pp. 1–1, 2015.

[3] I. Villar, L. Mir, I. Etxeberria-Otadui, J. Colmenero, X. Agirre, and T. Nieva, "Optimal design and experimental validation of a medium-frequency 400kva power transformer for railway traction applications," in *Energy Conversion Congress and Exposition (ECCE), 2012 IEEE*, Sept 2012, pp. 684–690.

[4] M. A. Bahmani, T. Thiringer, and H. Ortega, "An accurate pseudoempirical model of winding loss calculation in hf foil and round conductors in switchmode magnetics," *Power Electronics, IEEE Transactions on*, vol. 29, no. 8, pp. 4231–4246, Aug 2014.

[5] R. T. Naayagi, A. Forsyth, and R. Shuttleworth, "High-power bidirectional dc-dc converter for aerospace applications," *Power Electronics, IEEE Transactions on*, vol. 27, no. 11, pp. 4366–4379, 2012.

[6] M. A. Bahmani, "Design and optimization of hf transformers for high power dc-dc applications," Licentiate Thesis, Chalmers University of Technology, Gothenburg, Sweden, April 2014.

[7] R. De Doncker, D. Divan, and M. Kheraluwala, "A three-phase soft-switched high-power-density dc/dc converter for high-power applications," *Industry Applications, IEEE Transactions on*, vol. 27, no. 1, pp. 63–73, 1991.

[8] C. Meyer, "Key components for future offshore dc grids," Ph.D. dissertation, RWTH Aachen University, Germany, 2007.

[9] M. A. Bahmani, E. Agheb, T. Thiringer, H. K. Hoidalen, and Y. Serdyuk, "Core loss behavior in high frequency high power transformers—i: Effect of core topology," *Journal of Renewable and Sustainable Energy*, vol. 4, no. 3, p. 033112, 2012.

[10] M. A. Bahmani and T. Thiringer, "Accurate evaluation of leakage inductance in high frequency transformers using an improved frequency-dependent expression," *Power Electronics, IEEE Transactions on*, vol. PP, no. 99, pp. 1–1, 2014.

[11] W.-J. Gu and R. Liu, "A study of volume and weight vs. frequency for high-frequency transformers," in *Power Electronics Specialists Conference, 1993. PESC '93 Record., 24th Annual IEEE*, Jun 1993, pp. 1123–1129.